Influence of the stoichiometric ratio on the material properties and the aging behavior of anhydride-cured epoxy systems

Author(s):
Küchler, Florian; Färber, Raphael; Franck, Christian M

Publication date:
2023-11-02

Permanent link:
https://doi.org/10.3929/ethz-b-000625088

Originally published in:
Journal of Physics D: Applied Physics 56(44), https://doi.org/10.1088/1361-6463/acea8f

Influence of the stoichiometric ratio on the material properties and the aging behavior of anhydride-cured epoxy systems

Florian Küchler, Raphael Färber, Christian M. Franck

High Voltage Laboratory, ETH Zurich, 8092 Zurich, Switzerland

E-mail: kuechler@eeh.ee.ethz.ch

July 2023

Abstract. When partial discharge (PD) and dielectric heating effects can be excluded, comparatively little is known about the aging behavior of polymeric insulation materials under combined environmental and electric field stress. Since it was found in an earlier study that hygroelectrical stress leads to a strong reduction in the residual breakdown strength of anhydride-cured epoxy samples, the goal of this contribution is to determine if a material modification could enhance the insulation performance under hygroelectrical stress. For this purpose, epoxy samples of different stoichiometric ratios (SRs) were manufactured and hygroelectrically stressed. The material properties were evaluated by AC breakdown strength measurements as well as by Fourier-transform infrared (FTIR) spectroscopy before and after each aging sequence. Gravimetric analysis quantified the water diffusion behavior and the (steady-state) water absorption during exposure to different relative humidity (RH) levels at room temperature. The breakdown strength decreases for both increasing and decreasing SR compared to SR = 95 %. Moreover, FTIR measurements revealed that an increase of the SR leads to a higher amount of unreacted anhydride which correlates with an increasing amount of absorbed water. Thus, the mutual presence of water in the atmosphere and of unreacted anhydride in the epoxy material is identified as the main risk factor for epoxy degradation under the influence of electrical stress, since unreacted anhydride favors stronger water absorption and the presence of water inside the material is attributed to a lowering of the potential barrier for molecular bond breaking. Remarkably, the breakdown strength of non-aged samples is lower at SR = 80 % compared to SR = 95 %, but the long-term performance with respect to insulation aging is enhanced, which correlates with the non-/less-existing unreacted anhydride in the material.

1. Introduction

The recent progress in wide bandgap semiconductor technologies, namely in the development of silicon carbide (SiC) and gallium nitride (GaN) devices, paves the way for a growing number of power electronic applications in new areas. Power electronic components enable, for example, the integration of renewable energy sources

into modern electric grids [1, 2] by solid-state transformers (SSTs) [3]. Moreover, they provide increased efficiencies and power densities in space- or weight-critical areas, such as for traction [4], electric mobility [5] or electric aircraft [6] applications.

This is mainly achieved by the reduced switching losses due to increased switching speeds ($>10\,\mathrm{kV\,\mu s^{-1}}$) [7, 8] as well as by the higher power conversion densities due to increased switching frequencies ($>10\,\mathrm{kHz}$) [9], enabled by the novel SiC and GaN devices. In addition, their higher blocking voltages ($>2\,\mathrm{kV}$) allow for a growing number of medium-voltage (MV) and high-voltage (HV) applications [10].

However, the aforementioned advancements in semiconductor technologies come with challenges for the involved insulation systems, which need to perform reliably under the new type of electrical stresses, which are characterized by higher switching frequencies, increased switching speeds and higher voltage levels as well as by voltages consisting of different frequency components [11]. In this context, common risk factors for premature failures of polymeric insulation materials reported in literature are an enhanced partial discharge (PD) activity or dielectric heating [12].

Comparatively little is known about aging mechanisms of polymeric insulation in the absence of PDs and dielectric heating. Previous studies on this topic [13, 14] revealed a strong decrease in the residual breakdown strength of anhydride-cured epoxy samples, if, in addition to electric field stress (with the confirmed absence of PDs and dielectric heating), a high air humidity (leading to higher amount of absorbed water) was present.

These findings suggest to modify the used material in a way to reduce the water absorption in the presence of high air humidity in order to enhance the overall insulation performance under hygroelectric stress profiles. The frequently used approach of incorporating nanoparticles into the epoxy matrix is often associated with an increased water absorption tendency of the polymer (in particular at the polymer-nanoparticle-interfaces) [15, 16]. Hence, other methods are needed. For example, a fairly simple concept is the variation of the resin-to-hardener ratio, i.e the material composition does not necessarily need to exhibit a stoichiometric ratio (SR) [17]. The SR describes the ratio of chemical substances at which all substances/reactants have reacted completely, i.e. no excess of one (or more) of the substances exists after the reaction. It was demonstrated by [18] that, in doing so, it becomes possible to change the amount of the steady-state water absorption and thus the dielectric permittivity and the dielectric losses of the epoxy system.

Following this promising approach, the present contribution aims to show how the material properties and in particular the aging behavior (under hygroelectrical stress) of an anhydride-cured epoxy material can be modified by changing its stoichiometric ratio (or more precisely its resin-to-hardener ratio). Moreover, the goal of this study is to identify risk factors and to formulate requirements for aging-resistant epoxy insulation materials in the absence of PD activity and dielectric heating.

For this purpose, anhydride-cured epoxy samples of different resin-to-hardener ratios (in the following labeled as different SRs) were manufactured and afterwards hygroelectrically stressed under similar conditions as applied in earlier works [13, 14].

The assessment of the material properties before and after different aging sequences is similar to the analysis in [13], but only the Fourier-transform infrared (FTIR) spectra and the short-term AC breakdown strength (representing the material's residual breakdown strength) are used in this work. Additionally, the water absorption behavior of the epoxy samples was examined by means of gravimetrical analysis.

2. Methods

In this section, the manufacturing, preparation and conditioning procedure of the used epoxy samples is presented (section 2.1), before the procedures for water absorption measurements (section 2.2), hygroelectrical stressing (section 2.3), AC breakdown strength measurements (section 2.4) and FTIR measurements (section 2.5) are described.

2.1. Epoxy sample manufacturing, preparation and conditioning

All investigations in this work were carried out with a three-component epoxy system, provided as raw materials from ELANTAS consisting of a resin (DGEBA: 2,2-Bis(4-glycidyloxyphenyl)propane), an anhydride-based hardener (mainly THPA: tetrahydro-4-methylphthalic anhydride) as well as a catalyst (BDMA: benzyldimethylamine). Depending on the mixing ratios of the components, given in table 1, three different stoichiometric ratios (SRs) were obtained.

For the study of aging effects, a mold for recessed samples with a flat part of a diameter of 5 mm and a thickness of 200 µm in the middle of the sample was designed and employed, see figure 1 (a). The recessed shape allows, when coated with a metallic electrode, as shown in figure 1 (b), PD-free aging of the flat inner part. Strong evidence for the absence of PD-related aging with these silver-coated recessed samples can be found in an earlier work [13]. The effect of the metal coating with respect to the maximum electric field occurring inside the sample and at its surface is shown for a test peak voltage = 7.5 kV in figure 1 (c) by the electric field simulations carried out with COMSOL Multiphysics, since it leads to a uniform maximum electric field at the thinnest part of the sample, which was examined in the aging studies (see sections 2.3, 2.4 and 2.5) of this work. The mold design as well as the manufacturing procedure for the recessed samples is described in detail in [13].

As the recessed samples have a non-uniform thickness, they are not useful for water diffusion measurements (see section 2.2), which require flat and uniform samples of high aspect ratio (i.e. large area and small thickness) in order to achieve a uniform diffusion through the sample in reasonable time. For this purpose, a mold for vertical pouring of the liquid epoxy mixture with replaceable spacers of defined thickness (typically 500 µm as lower thicknesses were not suitable due to the brittleness of the epoxy samples) was designed and built. Note that such samples are not suitable for PD-free aging, because applying an electrode to the sample surface unavoidably creates a triple-point, favoring

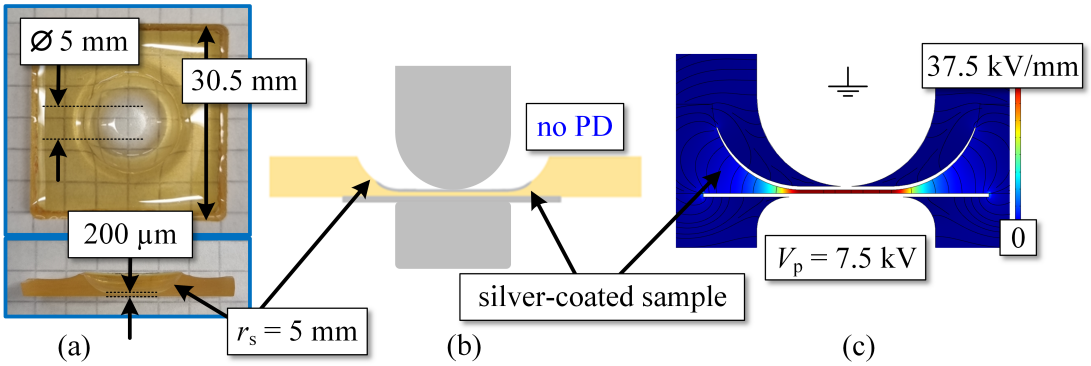

Figure 1: Top view, cross-section and dimensions of manufactured recessed epoxy samples (a) with schematic of the sample-electrode configuration used for aging in the absence of PDs (b) and the corresponding electric field simulation plot (c).

Table 1: Main components of the epoxy samples (DGEBA: 2,2-Bis(4-glycidyloxyphenyl)propane, THPA: tetrahydro-4-methylphthalic anhydride, BDMA: benzyldimethylamine) used within this work for different stoichiometric ratios (SRs), whereas the standard mixing ratio is depicted in bold (i.e. the majority of samples was manufactured with SR = 95 %).

		Share in wt% depending on SR		
Material class	Function	SR = 80%	**SR = 95%**	SR = 110%
DGEBA	resin	100	**100**	100
THPA (mainly)	hardener	72	**85**	99
BDMA	catalyst	0.5	**0.5**	0.5

PD inception at the thinnest sample part (due to the uniform thickness).

Manufacturing of both types of samples was carried out by mixing the components according to the ratios given in table 1 with a stirrer for 5 min under clean room conditions with subsequent degassing under vacuum (1...10 mbar) for 15 min. The molds were cleaned with ethanol and prepared with a silicone-based releasing agent (Huntsman QZ 13), before filling the mixture in the mold, followed again by degassing under vacuum (1...10 mbar) for 15 min. Afterwards, the samples were cured in an oven (6 h at 80 °C, then 6 h at 160 °C) and subsequently demolded. Some of the samples used in the present work were post-cured (PC), which represents an additional second curing cycle under the identical curing conditions mentioned above.

Preparation and conditioning of the samples before conducting experimental investigations included at first the cleaning with silicone cleaner (Silikon-EX 2609) in an ultrasonic bath for 10 min to remove residuals of the releasing agent, followed by cleaning with ethanol. The thickness of every single sample was measured by means of a precision measurement device (Sylvac Hi-Cal 300) with the inclusion criterion for the

sample thickness $d \in [190\,\mu\text{m}, 210\,\mu\text{m}]$. Afterwards, the samples were dried in an oven at 50 °C (according to ISO 62:2008 [19]) for >24 h and conditioned at the desired relative humidity (RH) level for >24 h. This was found sufficient for saturated (steady-state) water absorption, which was estimated to occur after 6.5 h in the 200 µm thick part of the recessed samples, based on water diffusion measurements on 500 µm thick samples with a uniform thickness, see section 2.2. For the recessed samples intended for aging tests, silver conductive paint (SCP Electrolube) was applied on both sides of the sample with subsequent conditioning for >24 h in the desired test atmosphere. Gravimetric measurements confirmed that the silver coating is permeable to water, see section 3.1.

2.2. Water absorption measurements

Water absorption was measured by means of gravimetric analysis with a high-precision scale (Kern ABT 100-5NM, with accuracy down to 0.01 mg). For this purpose, flat epoxy samples with a uniform thickness of $d = 500\,\mu\text{m}$ were dried according to section 2.1 and afterwards exposed to the desired level of relative humidity (RH) at ambient temperature (±22 °C). The circuit and procedure for the control of the RH level is illustrated and described detailed in figure 2 (b) and section 2.3, respectively.

The time-dependent amount of a diffusing substance Δm, such as water, in relation to the value at saturation Δm_{sat} (i.e. at infinite time) across the polymer sample thickness d is given by [20]

$$\frac{\Delta m(t)}{\Delta m_{\text{sat}}} = 1 - \frac{8}{\pi^2} \sum_{n=0}^{\infty} \frac{1}{(2n+1)^2} \exp\left(-\frac{D_{\text{d}}(2n+1)^2\pi^2 t}{d^2}\right). \tag{1}$$

For values of $\Delta m/\Delta m_{\text{sat}} < 0.6$, (1) can be simplified in order to calculate the diffusion coefficient D_{d} by using the initial slope $k = \Delta m/\sqrt{t}$, when displaying Δm as a function of $\sqrt{t}$ [21], according to

$$D_{\text{d}} = \frac{\pi^2}{16}\left(\frac{d}{\Delta m_{\text{sat}}}\right)^2 k^2. \tag{2}$$

The diffusion behavior depending on the time t was measured by taking out and weighing the sample three times after different time intervals. The mean value (out of the three measurements per time) of the weight (or mass) change Δm was recorded until at least a saturation value Δm_{sat} was reached and displayed as a function of $\sqrt{t}$. This allowed to calculate the diffusion coefficient D_{d} with the help of the initial slope $k = \Delta m/\sqrt{t}$ according to (2).

2.3. Hygroelectrical stress setup and procedure

Inverter-type electrical stress was synthesized by superimposing a low-frequency AC (50 Hz) sinusoidal voltage and a high-frequency, pulse-width-modulated (PWM, kHz range) voltage, which results in so-called mixed-frequency medium voltage (MF-MV) stress. The electrical circuit, whose main elements are the half-bridge circuit to generate

the PWM voltage, the AC voltage source and the coupling capacitor C_2 is shown in figure 2 (a) and described in detail in [13].

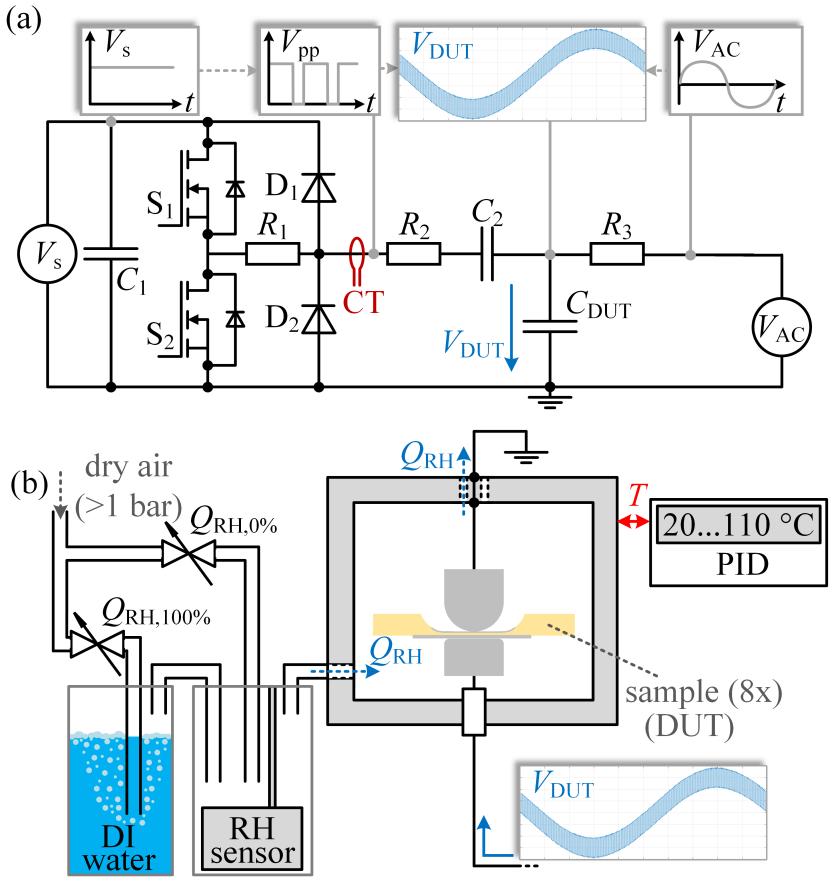

Figure 2: Schematic of the circuit of the mixed-frequency medium-voltage (MF-MV) stress setup used in this work (a). Schematic of the test cell with sample and electrode system as well as of the temperature and humidity control circuits (b).

The samples (up to eight in total) were placed inside a test cell with a temperature-controlled heating sleeve. Inside the test cell, the relative humidity (RH) can be varied within RH = 0...80 % at the ambient temperature $T = (22 \pm 1)\,°C$. The desired RH level was set by separating a dried air flow into two branches out of which one is directed into a mixing chamber with a RH sensor, while the other passes a bath of de-ionized (DI) water beforehand. By adjusting the volume flow of both branches, the RH level can be controlled, see figure 2 (b). Note that the same RH control approach was used for controlling the RH both inside the test cell as well as inside a sample storage box used for measuring the water absorption over time. The samples were conditioned according to the procedure described in section 2.1. Subsequently, they were placed inside individual sample holders, made of PTFE (for temperature stability) with holes for air passage, between two Aluminum electrodes with spring contacts for defined contact pressure. Effects of ozone (or other gases) generated during PD activity,

Table 2: Electrical stress conditions used in this work with the ambient conditions being RH = (75 ± 3) % and $T = (22 \pm 1)\,^{\circ}\mathrm{C}$.

$V_{\mathrm{AC,p}}/V_{\mathrm{PWM,pp}}/f_{\mathrm{PWM}}/D_{\mathrm{c}}$ in kV/kV/kHz/-	$V_{\mathrm{PWM,pp}}/\tau_{\mathrm{r}}$ in kV µs^{-1}	V_{p} in kV	V_{RMS} in kV	t_{d} in h
5.75/3.5/10/0.5	38.9	7.5	4.4	48
0/3.5/10/0.5	38.9	1.75	1.75	48

and hence potentially influencing the aging behavior [22], were excluded/minimized by the continuous, humidity-controlled air flow through the test cell. The RH values in this work are given as fixed values, e.g. RH = 75 %, even if slight differences (±3 %) cannot be fully excluded according to the specifications of the RH sensor (HTM2500LF).

The MF-MV stress conditions used in this work are given in table 2. Therein, $V_{\mathrm{AC,p}}$ represents the peak voltage of the sinusoidal AC voltage, $V_{\mathrm{PWM,pp}}$ the peak-to-peak PWM voltage, f_{PWM} the frequency of the rectangular pulses, D_{c} the duty cycle, $V_{\mathrm{PWM,pp}}/\tau_{\mathrm{r}}$ the slew rate with the pulse rise time τ_{r}. The voltages V_{p} and V_{RMS} denote the peak and the root-mean-square (RMS) voltage of the superimposed AC + PWM voltage waveform, respectively. Hygroelectrical stress was applied during the time duration t_{d}.

Analysis of the samples' health state was carried out by measuring the short-term AC breakdown strength (section 2.4) as well as the Fourier-transform infrared (FTIR) spectra (section 2.5) before and after each aging sequence.

2.4. AC breakdown strength measurements

The short term AC breakdown strength was measured (as described in detail in [13, 14]) according to IEC 60243-1 and ASTM D149 with a voltage ramp of $2\,\mathrm{kV\,s^{-1}}$ to reach the breakdown usually in 10...20 s [23, 24]. For this purpose, an AC (50 Hz) test voltage, fed via a high-voltage transformer, was used, whereas a digital storage oscilloscope (DSO) was triggered by a current transformer in the moment of breakdown, which enables the recording of the voltage waveform at the test object during breakdown and thus of the breakdown voltage and polarity. In order to prevent surface discharges, the test object (i.e. the silver-coated samples) were immersed in insulating oil (Shell Diala S4 ZX-1).

Small variations of the measured thickness $d_{\mathrm{meas}} \in [190\,\mu\mathrm{m}, 210\,\mu\mathrm{m}]$ were considered by relating d_{meas} to the nominal thickness $d_{\mathrm{n}} = 200\,\mu\mathrm{m}$ according to [24], which was experimentally verified in [14].

Statistical analysis of breakdown strength measurements was carried out by representing the data as box plots, consisting of median, boxes between the 25$^{\mathrm{th}}$ and 75$^{\mathrm{th}}$ percentiles with whiskers up to 1.5 times the interquartile distance. No values outside of this range were recorded.

2.5. Fourier-transform infrared (FTIR) spectroscopy measurements

As described also in [13], the chemical composition of the non-aged and aged materials was analyzed by means of Fourier-transform infrared (FTIR) spectroscopy. For the measurements in this work, a diamond attenuated total reflection (ATR) type instrument (Varian 640 Fourier Transform Infra Red Spectrometer) was used with scans (averaged out of 64 scans for each measurement) in the wavelength range of 750...4000 cm^{-1}. In the case of hygroelectrically stressed samples, the silver electrodes were removed with ethanol before each FTIR scan. It was confirmed by reference measurements (not shown here) that this procedure did not lead to measurable changes in the FTIR spectra.

In order to take into account potential variations of the absolute values of the measured absorbance between different FTIR scans, it is suggested to relate the scans to reference peaks which are known to be (almost) unaffected by aging. For anhydride-cured epoxy, the absorbance around 1608 cm^{-1} is reported to be the most stable during aging due to its correspondence to the aromatic structure in epoxy [25]. Thus, it is also considered as suitable reference peak in this work and all FTIR spectra were related to this absorbance peak.

3. Results

In this section, the results of water absorption, breakdown strength and FTIR measurements as well as the results of the conducted aging study are presented.

3.1. Water absorption measurements

Investigations on the water diffusion behavior and on the water absorption in the epoxy samples of different SRs were carried out by gravimetric analysis according to the procedure described in section 2.2. The weight increase due to water absorption Δm was measured over time t and displayed as a function of $\sqrt{t}$, resulting in figure 3. From these curves, it is evident that in all of the studied cases, the water diffusion follows the behavior described by Fick's law of diffusion. Moreover, figure 3 (a) shows that the amount of absorbed water clearly increases with the SR. The (steady-state) saturated water absorption levels Δm_{sat} are reached approximately after the same periods of time for different SRs and different RH values, with higher amount of saturated water absorption occurring at higher RH as seen from figure 3 (b).

The diffusion coefficient D_{d} was calculated with the help of the initial slope $k = \Delta m/\sqrt{t}$ according to (2), as can be seen from the results for samples of different stoichiometric ratios (SRs) at RH = 80 % in figure 3 (a). The calculated values of the diffusion coefficient D_{d} as well as the measured maximum saturated water absorption Δm_{sat} is given in table 3 for samples of different SRs at two different RH levels. The order of magnitude of the calculated diffusion coefficient appears to vary only slightly with no clear trend, indicating that water diffusion occurs on similar timescales for all

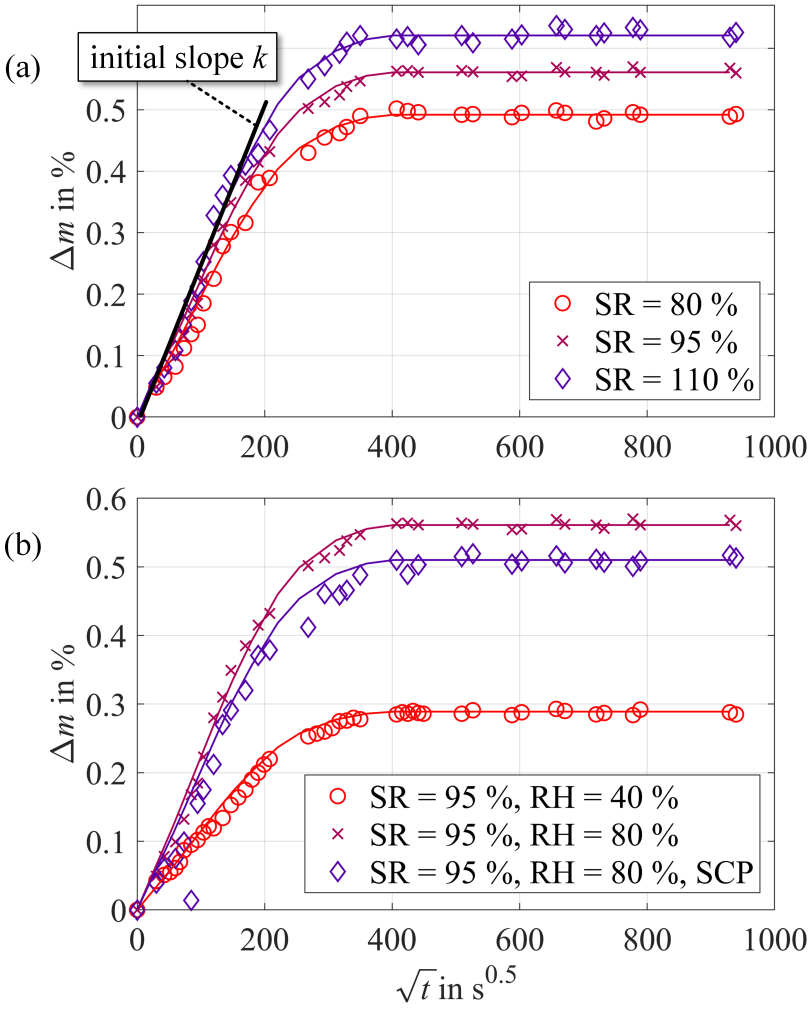

Figure 3: Measurement results of the weight change Δm of 500 µm thick epoxy samples over time, displayed as a function of $\sqrt{t}$ to determine the initial slope $k = \Delta m/\sqrt{t}$ for diffusion coefficient estimation: results for different stoichiometric ratios (SRs) at RH = 80 % (a) and for SR = 95 % at different RH levels, including samples with silver conductive paint (SCP) coating (b). The solid lines represent the best fit to Fick's law of diffusion.

SRs. With the help of the diffusion coefficients, the measured values can be fitted (as described in ISO 62:2008 [19]) according to Fick's law of diffusion, represented as solid lines in figure 3.

Moreover, measurements of samples coated with silver conductive paint (SCP) reveal similar diffusion behavior as without coating, as shown in figure 3 (b), indicating that the paint is permeable to water. Note that the small difference between the weight change of samples with and without coating in figure 3 (b) can be attributed to the different water absorption tendency of the material in which the silver particles are embedded (with a typical coating thickness of a few tens of µm) compared to epoxy.

The calculated diffusion coefficients were used to estimate with (2) the time until a

Table 3: Diffusion coefficients D_d estimated from water absorption measurements with (2) and measured maximum weight change Δm_sat (i.e. saturated, steady-state water absorption) of plane 500 µm thick epoxy samples at different levels of relative humidity (RH).

		Stoichiometric ratio (SR)		
Parameter	Unit	80 %	95 %	110 %
D_d at RH = 40 %	$10^{-9}\,\mathrm{cm^2\,s^{-1}}$	6.6	5.5	6.1
D_d at RH = 80 %	$10^{-9}\,\mathrm{cm^2\,s^{-1}}$	7	8.6	9.1
Δm_sat at RH = 40 %	%	0.25	0.29	0.33
Δm_sat at RH = 80 %	%	0.49	0.56	0.62

saturated (steady-state) water absorption is reached in the inner, thin (200 µm) part of the recessed epoxy samples. At RH = 80 %, this results in a time of $t_\mathrm{sat} \approx 6.5\,\mathrm{h}$. This confirms that the used conditioning times of >24 h were sufficient to reach a steady-state concentration of water inside the flat inner part (which solely is of interest with respect to aging) of the recessed epoxy samples.

3.2. AC breakdown strength measurements

For non-aged epoxy samples of in total three different SRs, the short-term AC breakdown strength was measured according to the procedure described in section 2.4. The results are displayed in figure 4 and show that the highest breakdown strength is achieved at SR = 95 %, i.e. for the base epoxy material used for the post-curing measurements in this work and for the aging studies presented in [13, 14].

3.3. Fourier-transform infrared (FTIR) spectroscopy measurements

FTIR spectra obtained for epoxy samples of different SRs are shown in figure 5. Characteristic differences are visible at the wavelength ranges between 850...1000 $\mathrm{cm^{-1}}$ and 1650...1950 $\mathrm{cm^{-1}}$. The reasons for these differences will be discussed in section 4. Note that the rather strongly varying peak around 2350 $\mathrm{cm^{-1}}$ is attributed to the atmospheric CO_2 concentration and thus not related to the epoxy material structure.

In figure 6, the FTIR spectra of two epoxy samples both after standard curing (i.e. after one curing cycle) as well as after post-curing (i.e. after two curing cycles) are shown with a focus on two characteristic wavelength ranges which are discussed in section 4.

3.4. Aging study results

MF-MV stressing of epoxy samples of different SRs at different RMS voltage levels (1.75 and 4.4 kV, see table 2 led to the residual breakdown strength values shown in

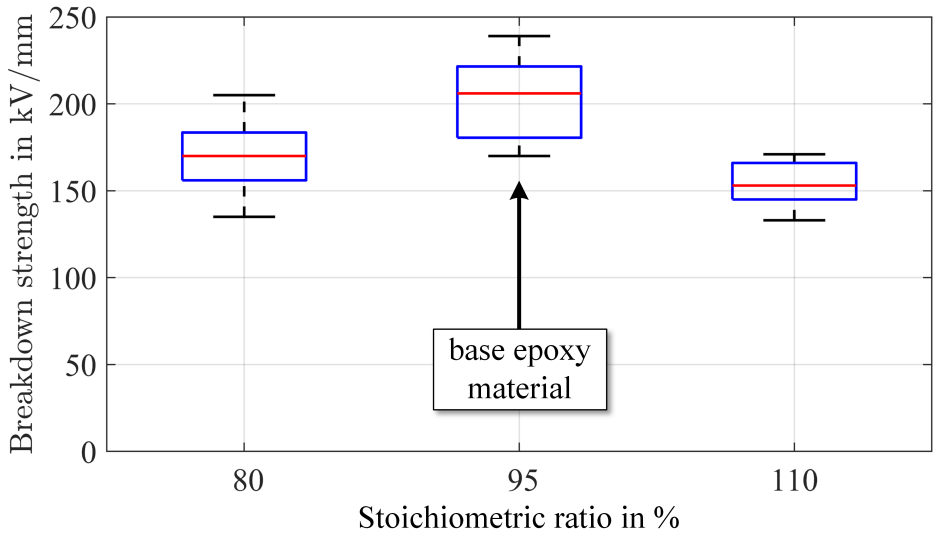

Figure 4: Short-term AC breakdown strength for non-aged epoxy samples with different stoichiometric ratios.

figure 7. The base material (i.e. SR = 95 %) exhibited a strong reduction in the breakdown strength due to the hygroelectrical stress, which was similarly observed for the material at higher SR (110 %). In contrast, the material with lower SR (80 %) shows no significant change in the breakdown strength for the studied stress conditions. Hygroelectrical aging at $V_{\mathrm{RMS}} = 4.4\,\mathrm{kV}$ of epoxy samples after post-curing (PC) led to a breakdown strength value similar as for non-aged samples.

It should be mentioned that the FTIR spectra of epoxy samples show no significant changes after aging for all of the three studied SRs (not shown here). This can be seen, for example, in [13] for the base material, i.e. SR = 95 %.

4. Discussion

It is expected that a higher amount of unreacted material components (i.e. in the present case either unreacted epoxide or anhydride) results in a lower breakdown strength of the cured material. This was observed also in figure 4, as the breakdown strength reduction of materials with a SR of 80 and 110 % compared to SR = 95 % can be explained by the higher amounts of unreacted material components (and thus a less dense molecular network), namely an excess of epoxide in the case of SR = 80 % and an excess of anhydride in the case of SR = 110 %. It is thus indicated that the higher the difference between the ideal SR = 100 % and the actual SR is, the lower the breakdown strength of the epoxy insulation gets.

The base epoxy material with SR = 95 % should ideally have a small excess in epoxide, but no anhydride should be present if all reactions have taken place during curing. However, the FTIR measurements in Figure 5 show that not only for SR = 110 %, but also for SR = 95 % a bulge-like local peak emerges around $1770\,\mathrm{cm}^{-1}$, a

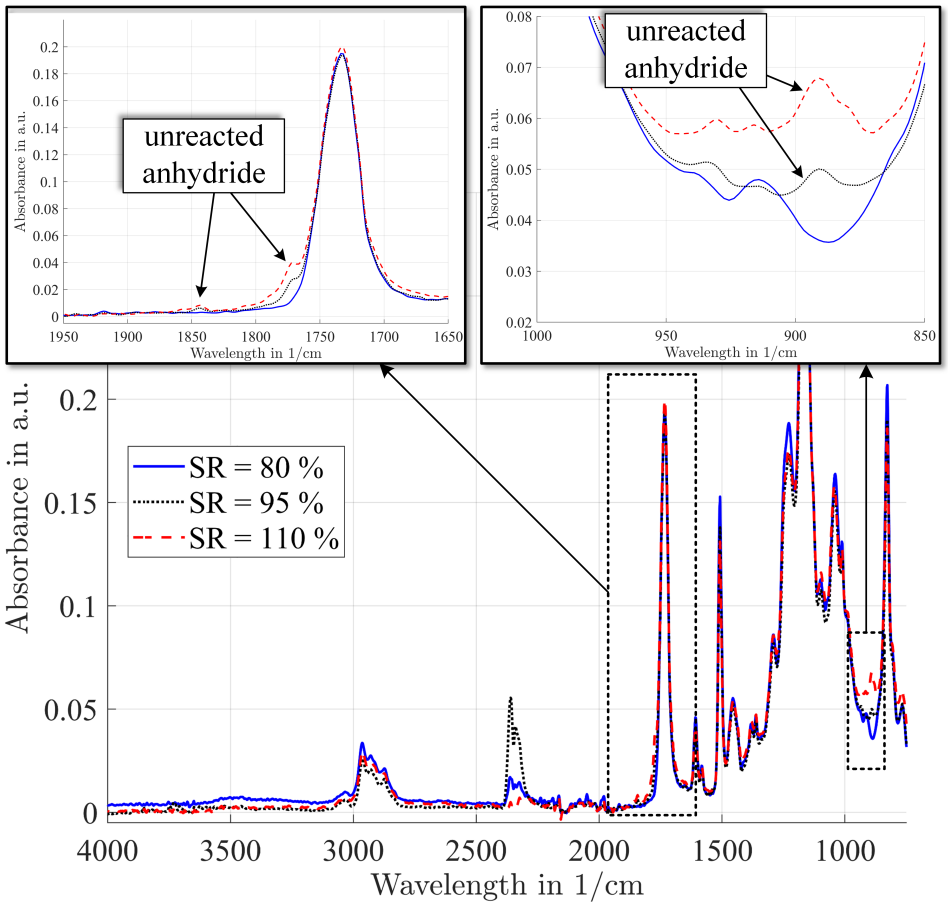

Figure 5: FTIR spectra of epoxy samples of different stoichiometric ratios (SRs) with focus on potential indications for unreacted anhydride.

small local peak emerges around 1840 cm^{-1} and a local peak is present around 890 cm^{-1}. By comparing these results with the results for anhydride-cured epoxy shown in [26, 27], it is evident that these local peaks correspond to the presence of unreacted anhydride. This indicates that for SR = 95 %, not all of the existing anhydride has fully reacted during curing. This is supported by the FTIR measurements of post-cured samples (figure 6), in which the aforementioned anhydride-related peaks have vanished, i.e. the reactions of remaining anhydride were completed due to the second curing cycle.

In figure 6, the increase in the broad peak around 3500 cm^{-1} which is associated with the hydroxyl group is an indicator for thermal aging, as was also observed by other authors [28, 29]. This is due to an increasing number of oxidation products which were created during thermal aging.

Moreover, it was found that post-curing had also a remarkable effect on the aging behavior of the epoxy samples under hygroelectrical stress as can be seen by the different residual breakdown strength values in figure 4. From these results, it appears that the absence of unreacted anhydride due to the post-curing prevents the material from aging in a way that is relevant for the electrical insulation performance (provided that the

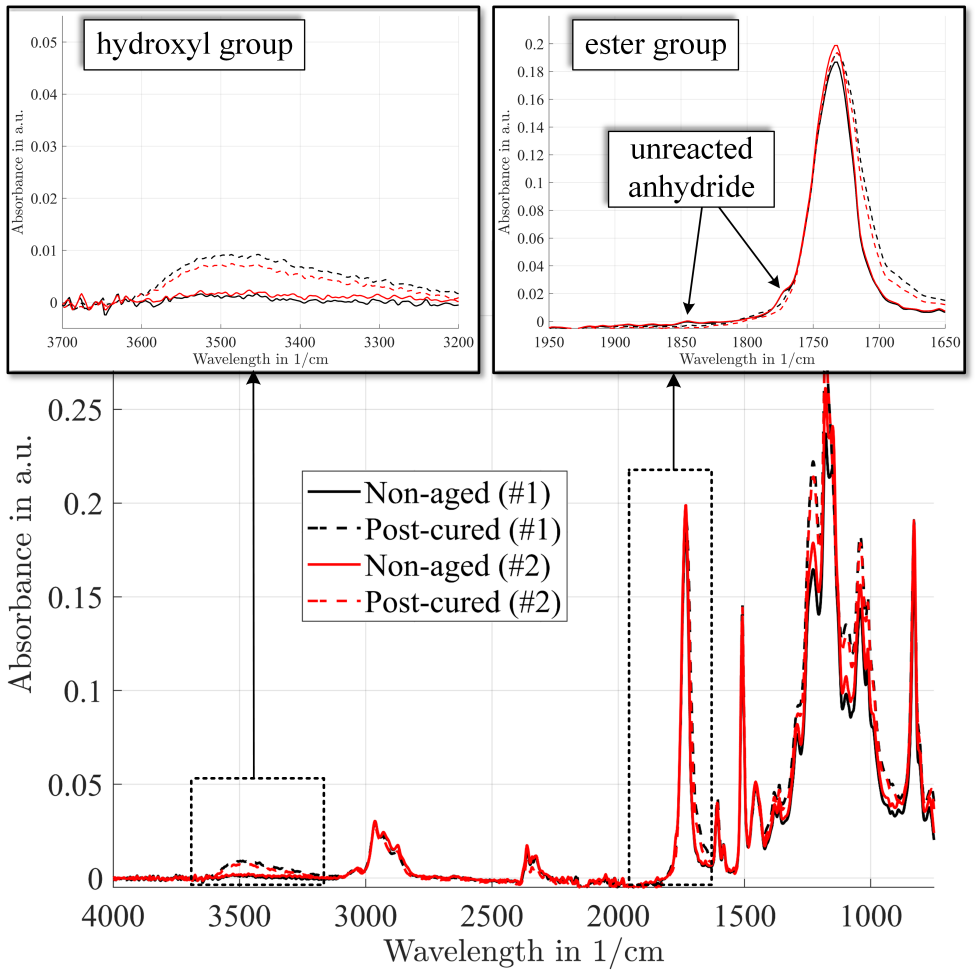

Figure 6: FTIR spectra of two epoxy samples (SR = 95 %) before and after post-curing (i.e. additionally cured by a second curing cycle) with focus on the hydroxyl and ester groups.

residual breakdown strength is the only or the most relevant aging marker). This is further supported by the results of the hygroelectrical stress study for different SRs shown in figure 4. Therein, only the material without any unreacted anhydride (see figure 5), i.e. for SR = 80 %, shows no reduction in the breakdown strength, but all other materials with a certain amount of unreacted anhydride exhibit a strong reduction in the residual breakdown strength. This is a noteworthy finding as it points out that samples with an excess in epoxide (but no unreacted anhydride) might have a lower breakdown strength before being stressed, but will be more stable when being exposed to hygroelectrical stress. However, if an elevated temperature is present during operation, a gradual post-curing might occur in service (given that enough reactants are present for the so far unreacted anhydride), which in turn could lead to an increased breakdown strength.

The finding made in an earlier work [13, 14] which show that (strong) aging occurs only under hygroelectrical stress, but not under pure electrical stress of the same

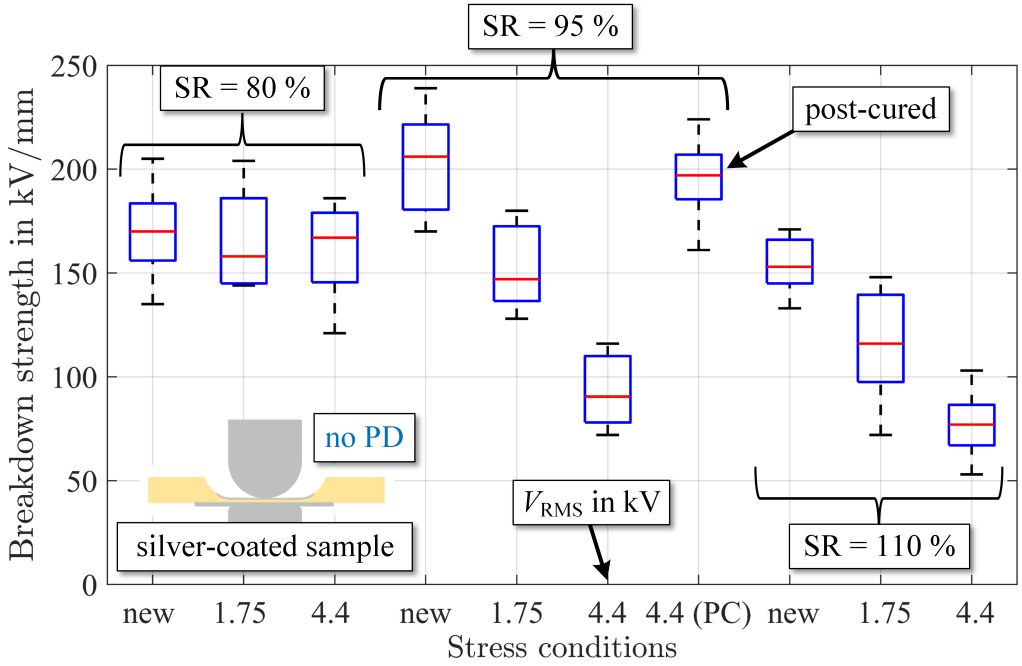

Figure 7: Influence of hygroelectrical stress at different RMS voltage levels (see table 2) as well as of post-curing (PC) with a second curing cycle and subsequent hygroelectrical stressing (at $V_{\mathrm{RMS}} = 4.4\,\mathrm{kV}$ and $\mathrm{RH} = 75\,\%$) on the residual breakdown strength of epoxy samples of different stoichiometric ratios (SRs).

voltage type and level indicates that the presence of absorbed water appears to initiate or accelerate the degradation. The water absorption measurements for different SRs (figure 3) clearly demonstrate that more water can be absorbed when more unreacted anhydride is present. The predominant aging mechanism under the test conditions of this work (i.e. in the absence of both partial discharges and dielectric heating) was proposed in [13, 14] to be of electromechanical origin. More precisely, it was hypothesized that the alternating electric field stress leads to a rearrangement of the free volume of the amorphous polymer, thus increasing locally the free path over which an electron can be accelerated by the electric field. This increases the probability of occurrence of high-energy electrons, which might be able to cause the breaking of molecular bonds. As it was found by [30] that the presence of water lowers the potential energy barrier to cause the breaking of molecular bonds, it can be assumed that the probability of bond breaking (and thus for irreversible aging) increases if more water can be absorbed due to the presence of unreacted anhydride.

In summary, the main risk factor for insulation aging for the epoxy material used in this work is identified as the mutual presence of water in the atmosphere and of unreacted anhydride in the epoxy material, favoring higher water absorption, which leads to an increasing probability of bond breaking under the influence of electric field stress.

5. Conclusion and outlook

The conclusions drawn from the presented study on the aging of epoxy samples modified by varying the stoichiometric ratio (SR) are summarized as follows:

- Increasing and decreasing the stoichiometric ratios both leads to a decrease in the breakdown strength compared to SR = 95 %.
- Increasing the stoichiometric ratio leads to a higher amount of unreacted anhydride which correlates with an increase in water absorption.
- The mutual presence of water in the atmosphere and of unreacted anhydride in the epoxy material is identified as the main risk factor for epoxy degradation under the influence of electrical stress, since unreacted anhydride favors a stronger water absorption and the presence of water in the material is attributed to a lowering of the potential barrier for molecular bond breaking.
- Unreacted anhydride is even present at SR = 95 % if the curing cycle is not fully completed. In this case, post-curing leads to the disappearance of both unreacted anhydride and of aging effects under hygroelectrical stress.
- At SR = 80 %, the breakdown strength of non-aged samples is lower as for SR = 95 %, but the long-term performance with respect to insulation aging (at room temperature) is enhanced, which is attributed to the non- or less-existing unreacted anhydride in the material.

Given the successful material modification with respect to the epoxy material performance under hygroelectrical stress profiles in the absence of PDs by reducing the tendency to absorb water (by lowering the SR), it appears promising to test additional material modifications which aim for an enhanced performance in the presence of water at similar hygroelectrical stress profiles. Similarly, enhancing the performance at higher temperatures might be a promising step to increase the durability under thermoelectrical stress profiles. Examples for different material modification approaches are the usage of additives, such as so-called functional network modifiers (FNMs) [31, 32] or the (widely investigated) incorporation of nanoparticles into the polymer matrix [33, 34, 35].

It has to be noted that the aforementioned material modifications mainly aim for an enhanced performance under PD-free stress conditions (i.e. Type I materials [36]). For this reason, materials which are to be used in the presence of PD activity (i.e. Type II materials [37]) need to be designed differently, e.g. by the (widely used) incorporation of mica tape into the polymer matrix, resulting in significantly increased path lengths to be covered by a discharge to cause an insulation breakdown.

Acknowledgments

The presented work is part of a project which is financially supported by ALTANA AG, Germany. The authors would like to thank Ralf Hoffmann, Fabio Campanini, Mattia Ferraris and Christian Schaumberg from ELANTAS/ALTANA AG, for the valuable

discussions and for providing the raw materials (resin, hardener, catalyst) for the used epoxy samples. In addition, the authors want to thank Yang Yao and Raffaele Mezzenga from the Laboratory of Food and Soft Materials, ETH Zurich for the possibility to use the FTIR setup as well as for the helpful support with performing the measurements.

6. References

[1] Huang A Q, Crow M L, Heydt G T, Zheng J P and Dale S J 2011 The future renewable electric energy delivery and management (FREEDM) system: The energy Internet *Proc. IEEE* **99** 133-148

[2] Tan D 2015 Emerging System Applications and Technological Trends in Power Electronics: Power electronics is increasingly cutting across traditional boundaries *IEEE Power Electron. Mag.* **2** 38-47

[3] Huber J E and Kolar J W 2016 Solid-State Transformers: On the Origins and Evolution of Key Concepts *IEEE Ind. Electron. Mag.* **10** 19-28

[4] Kolar J W and Ortiz G 2014 Solid-State-Transformers: Key Components of Future Traction and Smart Grid Systems *Proc. IEEE Intern. Power Electronics Conf.* **7**

[5] Aghabali I, Bauman J, Kollmeyer P J, Wang Y, Bilgin B and Emadi A 2021 800-V Electric Vehicle Powertrains: Review and Analysis of Benefits, Challenges, and Future Trends *IEEE Trans. Transport. Electrific.* **7** 927-948

[6] Madonna V, Giangrande P and Galea M 2018 Electrical Power Generation in Aircraft: Review, Challenges, and Opportunities *IEEE Trans. Transp. Electrific.* **4** 646-659

[7] Ji S, Zheng S, Wang F and Tolbert L M 2018 Temperature-Dependent Characterization, Modeling and Switching Speed Limitation Analysis of Third Generation 10 kV SiC MOSFET *IEEE Trans. Power Electron.* **33** 4317-4327

[8] Oswald N, Anthony P, McNeill N and Stark B H 2014 An Experimental Investigation of the Tradeoff between Switching Losses and EMI Generation With Hard-Switched All-Si, Si-SiC, and All-SiC Device Combinations *IEEE Trans. Power Electron.* **29** 2393-2407

[9] Wang Y, Lucia O, Zhang Z, Gao S, Guan Y and Xu D 2020 A Review of High Frequency Power Converters and Related Technologies *IEEE Open J. Indust. Electron. Soc.* **1** 247-260

[10] Okumura H 2015 A roadmap for future wide bandgap semiconductor power electronics *MRS Bulletin* **40** 439–444

[11] Mirza A Y, Bazzi A, Nguyen H H and Cao Y 2022 Motor Stator Insulation Stress Due to Multilevel Inverter Voltage Output Levels and Power Quality *Energies* **15** 1-18

[12] Stone G C and Culbert I 2014 Review of Stator Insulation Problems in Medium Voltage Motors Fed from Voltage Source PWM Drives *Proc. Int. Symp. Electr. Insul. Mat.* 50-53

[13] Küchler F, Färber R, Bill F, Renggli S and Franck C M 2023 Mixed-frequency medium-voltage aging analysis of epoxy in the absence of partial discharges and dielectric heating *J. Phys. D: Appl. Phys.* **56**

[14] Küchler F, Färber R, Šefl O, Bill F and Franck C M 2023 Influence of mixed-frequency medium-voltage and environmental stress on aging of epoxy *J. Phys. D: Appl. Phys.* **56**

[15] Zou C, Fothergill J G and Rowe S W 2008 The Effect of Water Absorption on the Dielectric Properties of Epoxy Nanocomposites *IEEE Trans. Dielectr. Electr. Insul.* **15** 106-117

[16] Alhabill F N, Ayoob R, Andritsch T and Vaughan A S 2018 Introducing particle interphase model for describing the electrical behaviour of nanodielectrics *Materials Design* **158** 62-73

[17] Alhabill F N, Ayoob R, Andritsch T and Vaughan A S 2017 Effect of resin/hardener stoichiometry on electrical behavior of epoxy networks *IEEE Trans. Dielectr. Electr. Insul.* **24** 3739-3749

[18] Alhabill F N, Andritsch T and Vaughan A S 2017 On Water Absorption and its Impact on the Dielectric Spectra of Epoxy Network with Different Stoichiometries *IEEE Conf. Electr. Insul. Dielectr. Phenom.*

[19] ISO 62:2008 2008 *Plastics - Determination of water absorption* (Int. Standard) vol 3
[20] Maffezzoli A M, Peterson L, Seferis J C, Kenny J and Nicolais L 1993 Dielectric characterization of water sorption in epoxy resin matrices *Polym. Eng. Sci.* **33** 75-82
[21] Crank J 1975 *The Mathematics of Diffusion* (Oxford University Press)
[22] Guastavino F and Ratto A 2012 Comparison Between Conventional and Nanofilled Enamels Under Different Environmental Conditions *IEEE Electr. Insul. Mag.* **28** 35-41
[23] IEC 60243-1:2013 2013 *Electrical strength of insulating materials - Test methods - Part 1: Test at power frequencies* (Int. Standard) vol 3
[24] ASTM D149-09 2013 *Standard Test Method for Dielectric Breakdown Voltage and Dielectric Strength of Solid Electrical Insulating Materials at Commercial Power Frequencies* (Americ. Nat. Standard)
[25] Andersson J, Gubanski S M and Hillborg H 2008 Properties of Interfaces between Silicone Rubber and Epoxy *IEEE Trans. Dielectr. Electr. Insul.* **15** 1360-1367
[26] Flores M, Fernandez-Francos X, Ramis X and Serra A 2012 Novel epoxy-anhydride thermosets modified with a hyperbranched polyester as toughness enhancer. I. Kinetics study *Thermochim. Acta* **544** 17-26
[27] Awais M, Chen X, Dai C, Meng F B, Paramane A and Tanaka Y 2021 Tuning Epoxy for Medium Frequency Transformer Application: Resin Optimization and Characterization of Nanocomposites at High Temperature *IEEE Trans. Dielectr. Electr. Insul.* **28** 1751-1758
[28] Delor-Jestin F, Drouin D, Cheval P-Y and Lacoste J 2006 Thermal and photochemical ageing of epoxy resin - Influence of curing agents *Polym. Degrad. Stab.* **91** 1247-1255
[29] Bordeori M M and Gupta N 2022 Electrochemical Changes in Epoxy Resin Due to Thermal Aging and Their Effect on Electrical Tree Growth *IEEE Trans. Dielectr. Electr. Insul.* **29** 1940-1947
[30] Parpal J-L, Crine J-P and Dang C 1997 Electrical Aging of Extruded Dielectric Cables - A Physical Model *IEEE Trans. Dielectr. Electr. Insul.* **4** 197-209
[31] Saeedi I A, Andritsch T and Vaughan A S 2019 On the Dielectric Behavior of Amine and Anhydride Cured Epoxy Resins Modified Using Multi-Terminal Epoxy Functional Network Modifier *Polymers* **11** 1-18
[32] Saeedi I A, Vaughan A S and Andritsch T 2019 Functional design of epoxy-based networks: Tailoring advanced dielectrics for next-generation energy systems *J. Phys. D. Appl. Phys.* **51**
[33] Tanaka T 2005 Dielectric nanocomposites with insulating properties *IEEE Trans. Dielectr. Electr. Insul.* **12** 914-928
[34] Zhao H, and Li R K Y 2008 Effect of water absorption on the mechanical and dielectric properties of nano-alumina filled epoxy nanocomposites *Compos. Part A Appl. Sci. Manuf.* **39** 602–611
[35] Awais M, Chen X, Dai C, Wang Q, Meng F-B, Hong Z, Paramane A and Tanaka Y 2022 Investigating optimal region for thermal and electrical properties of epoxy nanocomposites under high frequencies and temperatures *Nanotechnology* **33** 1-12
[36] IEC 60034-18-41 2014 *Rotating electrical machines – Part 18-41: Partial discharge free electrical insulation systems (Type I) used in rotating electrical machines fed from voltage converters – Qualification and quality control tests* (Int. Standard)
[37] IEC 60034-18-42 2017 *Rotating electrical machines – Part 18-42: Partial discharge resistant electrical insulation systems (Type II) used in rotating electrical machines fed from voltage converters – Qualification tests* (Int. Standard)